Contents lists available at ScienceDirect

Results in Physics

Hiemenz flow over a shrinking sheet in a hybrid nanofluid

Iskandar Waini[a,b], Anuar Ishak[b,*], Ioan Pop[c]

[a] *Fakulti Teknologi Kejuruteraan Mekanikal dan Pembuatan, Universiti Teknikal Malaysia Melaka, Hang Tuah Jaya, 76100 Durian Tunggal, Melaka, Malaysia*
[b] *Department of Mathematical Sciences, Faculty of Science and Technology, Universiti Kebangsaan Malaysia, 43600 UKM Bangi, Selangor, Malaysia*
[c] *Department of Mathematics, Babeş-Bolyai University, 400084 Cluj-Napoca, Romania*

ARTICLE INFO

ABSTRACT

This study investigates the Hiemenz flow of hybrid nanofluid over a shrinking sheet. The similarity equations are obtained using similarity variables and then solved using the bvp4c solver. The outcomes showed that dual solutions occur for the shrinking case, in the range of $-1.24657 < \lambda \leq -1.1$ with $\lambda_c = -1.24657$ is the point of bifurcation between the solutions. Meanwhile, the solution is unique for $\lambda > -1.1$. Besides, the heat transfer rate is intensified with the rise of hybrid nanoparticles. Moreover, as hybrid nanoparticles increases, the friction on the surface is increased for $\lambda < 1$, while it is decreased for $\lambda > 1$, and no friction occurs when $\lambda = 1$. Finally, these solutions are tested using the stability analysis where the outcomes found that the first solution is stable and acceptable.

Introduction

Historically, there are several types of boundary layer flow problems that have been developed in a fluid dynamic field, for example, the stagnation point flow. The stagnation point of the fixed surface in the boundary layer flow problem was initially explored by Hiemenz [1], and extended by Homann [2] to the case of the axisymmetric flow. Ariel [3] considered the hydromagnetic effects on the flow field where an analytical solution is obtained for the problem. Moreover, Wang [4] reported the flow on a shrinking sheet, and then this work was extended by Ishak et al. [5] to the case of the micropolar fluid. Further, the Hiemenz flow problems with several effects are also considered by numerous researchers [6–10].

Previously, most industrial processes use regular fluid in their cooling systems. However, an advanced fluid termed as 'nanofluid' given by Choi and Eastman [11], could enhance the fluid's heat transfer rate. Nanofluid consists of a single nanoparticle that suspended in the base fluid. The utilizing of nanofluid in heat transfer enhancement is considered by several researchers [12–17]. Furthermore, studies have shown that a significant increment in the heat transfer rate of nanofluid is attained when the hybrid nanoparticle is employed. The experimental works by Turcu et al. [18] and Jana et al. [19] were the earlier studies that utilizing the hybrid nanoparticles. Besides, Suresh et al. [20] conducted the experimental work using Al_2O_3–Cu hybrid nanoparticle to study the enhancement of the fluid thermal conductivity.

Apart from that, Devi and Devi [21] studied the flow over a

stretching surface containing Al_2O_3–Cu/water with MHD effects. The new mathematical correlations of hybrid nanofluid are introduced in their studies and found that the results from the modeling data and experimental data of Suresh et al. [20] are in good agreement. Then, Ghalambaz et al. [22] consider the stagnation point flow of Al_2O_3–Cu/water hybrid nanofluid towards a vertical plate. The flow over a wedge considered by Hassan et al. [23] and Mahanthesh et al. [24] with Cu-Ag and MoS_2-Ag hybrid nanoparticles, respectively. Besides, Waini et al. [25–29] inspected the dual solutions of the hybrid nanofluid flow. Also, the problem is continuously studied by various researchers [30–36] with various physical conditions. Additionally, the review papers of nanofluid [37–40] and hybrid nanofluid [41–47] can be found in the literature for further reading. Apart from that, some studies in the field of fluid mechanics can be found in Refs. [48–50].

Thus, we consider the Hiemenz flow over a shrinking sheet with the effect of hybrid nanoparticles (Al_2O_3-Cu). Besides, the dual solutions are attained and their stabilities are determined by the stability analysis. The numerical results are displayed in tables and figures, and then will be discussed theoretically.

Mathematical formulation

The Hiemenz flow of a hybrid nanofluid on a stretching/shrinking surface is considered. The flow configuration of the problem is illustrated in Fig. 1. Here, the free stream velocity is taken as $u_e(x) = U_e x$, while the surface velocity is $u_w(x) = U_w x$ with U_e and U_w are constants.

---

* Corresponding author.
 E-mail address: anuar_mi@ukm.edu.my (A. Ishak).
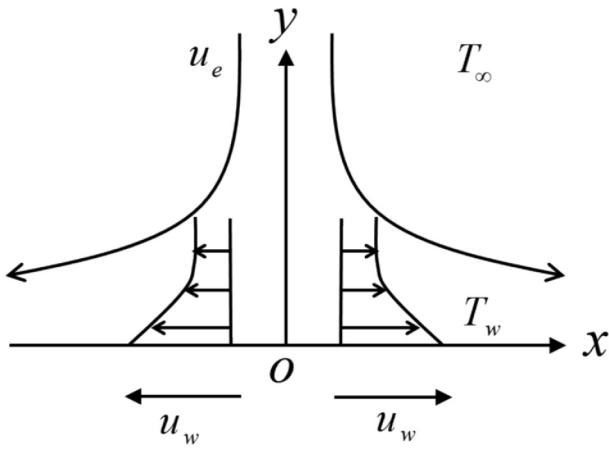
(a) Stretching surface
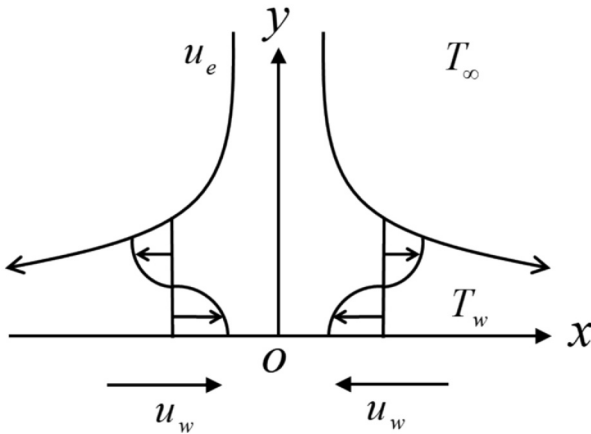
(b) Shrinking surface

Fig. 1. The flow configuration.

The ambient T_∞ and the surface T_w temperatures are also constants. Therefore, the governing equations are (see Ariel [3], Tiwari and Das [13], Devi and Devi [21]):

$$\frac{\partial u}{\partial x} + \frac{\partial v}{\partial y} = 0,$$

(1)

$$u\frac{\partial u}{\partial x} + v\frac{\partial u}{\partial y} = u_e \frac{du_e}{dx} + \frac{\mu_{hnf}}{\rho_{hnf}}\frac{\partial^2 u}{\partial y^2},$$

(2)

$$u\frac{\partial T}{\partial x} + v\frac{\partial T}{\partial y} = \frac{k_{hnf}}{(\rho C_p)_{hnf}}\frac{\partial^2 T}{\partial y^2},$$

(3)

subject to:

$$v = 0, \quad u = u_w(x), \quad T = T_w,$$
$$u \to u_e(x), \quad T \to T_\infty \quad \text{as} \quad y \to \infty$$

(4)

where the velocity components along the x- and y-axes are represented by u and v, and the temperature is given by T. Further, Table 1 presents the thermophysical correlations of nanofluid [14] and hybrid nanofluid [21]. Meanwhile, Table 2 displays the properties of nanoparticles and water [14]. Note that Al_2O_3 (subscripts $p1$) and Cu (subscripts $p2$) are the nanoparticles and their volume fractions are symbolised by φ_1 and φ_2, respectively. Moreover, the subscripts f, nf, and hnf are represent the fluid, nanofluid, and hybrid nanofluid, respectively.

Considering the following dimensionless variables (see White [51]):

$$\psi = (U_e \nu_f)^{1/2} x f(\eta), \quad \theta(\eta) = \frac{T - T_\infty}{T_w - T_\infty}, \quad \eta = (U_e/\nu_f)^{1/2} y,$$

(5)

where ν_f is the fluid kinematic viscosity and the stream function ψ is defined as $u = \partial\psi/\partial y$ and $v = -\partial\psi/\partial x$. Then, Eq. (1) is identically satisfied and one gets:

$$u = U_e x f'(\eta), \quad v = -(U_e \nu_f)^{1/2} f(\eta),$$

(6)

Thus, Eqs. (2) and (3) become:

$$\frac{\mu_{hnf}/\mu_f}{\rho_{hnf}/\rho_f} f''' + ff'' + 1 - f'^2 = 0,$$

(7)

$$\frac{1}{\Pr}\frac{k_{hnf}/k_f}{(\rho C_p)_{hnf}/(\rho C_p)_f}\theta'' + f\theta' = 0,$$

(8)

subject to:

$$f(0) = 0, \quad f'(0) = \lambda, \quad \theta(0) = 1,$$
$$f'(\eta) \to 1, \quad \theta(\eta) \to 0 \quad \text{as} \quad \eta \to \infty.$$

(9)

where the Prandtl number $\Pr$ and the stretching/shrinking parameter λ are defined as [52]

$$\Pr = \frac{(\mu C_p)_f}{k_f}, \quad \lambda = \frac{U_w}{U_e},$$

(10)

with $\lambda > 0$ and $\lambda < 0$ indicate the stretching and shrinking cases, respectively, while $\lambda = 0$ indicates the rigid surface. Note that for $\varphi_1 = \varphi_2 = 0$ (regular fluid) and $\lambda = 0$ (rigid surface), Eq. (7) reduces to those of the classical Hiemenz problem, see White [51].

The physical quantities of interest are the skin friction coefficients C_f and the local Nusselt number Nu_x which are defined as

$$C_f = \frac{\mu_{hnf}}{\rho_f u_e^2}\left(\frac{\partial u}{\partial y}\right)_{y=0}, \quad Nu_x = -\frac{xk_{hnf}}{k_f(T_w - T_\infty)}\left(\frac{\partial T}{\partial y}\right)_{y=0},$$

(11)

where the surface shear stress τ_w and the surface heat flux q_w are respectively given by

$$\tau_w = \mu_{hnf}\left(\frac{\partial u}{\partial y}\right)_{y=0}, \quad q_w = -k_{hnf}\left(\frac{\partial T}{\partial y}\right)_{y=0}.$$

(12)

Using (5), (11) and (12), we get

$$Re_x^{1/2} C_f = \frac{\mu_{hnf}}{\mu_f}f''(0), \quad Re_x^{-1/2} Nu_x = -\frac{k_{hnf}}{k_f}\theta'(0),$$

(13)

where the local Reynolds number is $Re_x = u_e x/\nu_f$.

Temporal stability analysis

Results show that Eqs. (7)–(9) admit the dual solutions for several physical parameters: one corresponding to the first solution and the other is the second solution. Consequently, the temporal stability analysis is required to determine the stable solution in the long run (see Merkin [53]; Weidman et al. [54]). To do this, we consider the unsteady case of Eqs. (2) and (3), where Eq. (1) remains unchanged.

$$\frac{\partial u}{\partial t} + u\frac{\partial u}{\partial x} + v\frac{\partial u}{\partial y} = u_e \frac{du_e}{dx} + \frac{\mu_{hnf}}{\rho_{hnf}}\frac{\partial^2 u}{\partial y^2},$$

(14)

$$\frac{\partial T}{\partial t} + u\frac{\partial T}{\partial x} + v\frac{\partial T}{\partial y} = \frac{k_{hnf}}{(\rho C_p)_{hnf}}\frac{\partial^2 T}{\partial y^2}.$$

(15)

Based on Eq. (5), the new variables are given as follows:

$$\psi = (U_e \nu_f)^{1/2} x f(\eta, \tau), \quad \theta(\eta, \tau) = \frac{T - T_\infty}{T_w - T_\infty},$$
$$\eta = (U_e/\nu_f)^{1/2} y, \quad \tau = U_e t,$$

(16)

Substituting (16) into (14) and (15), after linearization, one gets

Table 1

Thermophysical properties of nanofluid and hybrid nanofluid.

Properties	Nanofluid	Hybrid nanofluid
Dynamic viscosity	$\mu_{nf} = \dfrac{\mu_f}{(1-\varphi_1)^{2.5}}$	$\mu_{hnf} = \dfrac{\mu_f}{(1-\varphi_1)^{2.5}(1-\varphi_2)^{2.5}}$
Density	$\rho_{nf} = (1-\varphi_1)\rho_f + \varphi_1\rho_{p1}$	$\rho_{hnf} = (1-\varphi_2)[(1-\varphi_1)\rho_f + \varphi_1\rho_{p1}] + \varphi_2\rho_{p2}$
Heat capacity	$(\rho C_p)_{nf} = (1-\varphi_1)(\rho C_p)_f + \varphi_1(\rho C_p)_{p1}$	$(\rho C_p)_{hnf} = (1-\varphi_2)[(1-\varphi_1)(\rho C_p)_f + \varphi_1(\rho C_p)_{p1}] + \varphi_2(\rho C_p)_{p2}$
Thermal conductivity	$\dfrac{k_{nf}}{k_f} = \dfrac{k_{p1} + 2k_f - 2\varphi_1(k_f - k_{p1})}{k_{p1} + 2k_f + \varphi_1(k_f - k_{p1})}$	$\dfrac{k_{hnf}}{k_{nf}} = \dfrac{k_{p2} + 2k_{nf} - 2\varphi_2(k_{nf} - k_{p2})}{k_{p2} + 2k_{nf} + \varphi_2(k_{nf} - k_{p2})}$ where $\dfrac{k_{nf}}{k_f} = \dfrac{k_{p1} + 2k_f - 2\varphi_1(k_f - k_{p1})}{k_{p1} + 2k_f + \varphi_1(k_f - k_{p1})}$

Table 2

Thermophysical properties of nanoparticles and water.

Properties	Al_2O_3	Cu	water
$C_p \, (J/kgK)$	765	385	4179
$\rho \, (kg/m^3)$	3970	8933	997.1
$k \, (W/mK)$	40	400	0.613
Prandtl number, Pr			6.2

$$\frac{\mu_{hnf}/\mu_f}{\rho_{hnf}/\rho_f}\frac{\partial^3 f}{\partial\eta^3} + f\frac{\partial^2 f}{\partial\eta^2} + 1 - \left(\frac{\partial f}{\partial\eta}\right)^2 - \frac{\partial^2 f}{\partial\eta\partial\tau} = 0, \tag{17}$$

$$\frac{1}{\text{Pr}}\frac{k_{hnf}/k_f}{(\rho C_p)_{hnf}/(\rho C_p)_f}\frac{\partial^2\theta}{\partial\eta^2} + f\frac{\partial\theta}{\partial\eta} - \frac{\partial\theta}{\partial\tau} = 0. \tag{18}$$

The boundary conditions are

$$f(0,\tau) = 0, \quad \frac{\partial f}{\partial\eta}(0,\tau) = \lambda, \quad \theta(0,\tau) = 1,$$

$$\frac{\partial f}{\partial\eta}(\eta,\tau) \to 1, \quad \theta(\eta,\tau) \to 0 \quad \text{as} \quad \eta \to \infty. \tag{19}$$

Then, the steady solution $f = f_0(\eta)$ and $\theta = \theta_0(\eta)$ of Eqs. (7)–(9) are perturbed by the perturbation functions as follows (see Weidman et al. [54]):

$$f(\eta,\tau) = f_0(\eta) + e^{-\gamma\tau}F(\eta),$$
$$\theta(\eta,\tau) = \theta_0(\eta) + e^{-\gamma\tau}G(\eta), \tag{20}$$

where $F(\eta)$ and $G(\eta)$ are comparatively small compared to $f_0(\eta)$ and $\theta_0(\eta)$. By employing Eq. (20), Eqs. (17 and 18) become:

$$\frac{\mu_{hnf}/\mu_f}{\rho_{hnf}/\rho_f}F''' + f_0 F'' + f_0'' F - 2f_0' F' + \gamma F' = 0, \tag{21}$$

$$\frac{1}{\text{Pr}}\frac{k_{hnf}/k_f}{(\rho C_p)_{hnf}/(\rho C_p)_f}G'' + f_0 G' + \theta_0' F + \gamma G = 0, \tag{22}$$

subject to:

$$F(0) = 0, \quad F'(0) = 0, \quad G(0) = 0,$$
$$F'(\eta) \to 0, \quad G(\eta) \to 0 \quad \text{as} \quad \eta \to \infty. \tag{23}$$

Following Harris et al. [55], without loss of generality, we set the value $F''(0) = 1$ to obtain the eigen values γ.

Results and discussion

Now, the numerical computations are conducted using the bvp4c solver (see Shampine et al. [56]). The convergence of the solution strictly depends on the boundary layer thickness ($\eta \to \infty$) and the initial guess. This convergence issue is also influenced by the value of the selected parameters. The numerical procedures are explained as follows: First, Eqs. (7) and (8) are reduced to a system of ordinary differential equations of the first order. Now, Eq. (7) can be written as:

$$f = y(1), \quad f' = y'(1) = y(2), \tag{24a}$$

$$f'' = y'(2) = y(3), \tag{24b}$$

$$f''' = y'(3) = -\frac{\rho_{hnf}/\rho_f}{\mu_{hnf}/\mu_f}(y(1)y(3) + 1 - y(2)^2), \tag{24c}$$

while Eq. (8) reduces to:

$$\theta = y(4), \quad \theta' = y'(4) = y(5), \tag{25a}$$

$$\theta'' = y'(5) = -\text{Pr}\frac{(\rho C_p)_{hnf}/(\rho C_p)_f}{k_{hnf}/k_f}y(1)y(5), \tag{25b}$$

and the boundary condition (9) becomes:

$$y_a(1) = 0, \quad y_a(2) = \lambda, \quad y_a(4) = 1,$$
$$y_b(2) \to 1, \quad y_b(4) \to 0. \tag{26}$$

where the subscript a denotes the condition at the surface and the subscript b denotes the condition at the free stream. Then, Eqs. (24) to (26) are coded in Matlab software and their solutions are obtained by the bvp4c solver. The solver will then run and the outcomes are printed out as numerical values and graphs.

Note that the classical Hiemenz problem can be obtained by taking $\varphi_1 = \varphi_2 = 0$ (regular fluid) and $\lambda = 0$ (rigid surface). For this special case, we obtain the value of $f''(0) = 1.232588$. This result is comparable to those reported by Wang [4] and Bachok et al. [6]. Besides, the comparison values of $f''(0)$ for several λ when $\varphi_1 = \varphi_2 = 0$ are also provided in Table 3. The present results are satisfactory with the mentioned literature. Moreover, the values of $Re_x^{1/2}C_f$ and $Re_x^{-1/2}Nu_x$ under various parameters when Pr = 6.2 are calculated and presented in Table 4. For the case of rigid surface ($\lambda = 0$), it shows that the values of $Re_x^{1/2}C_f$ and $Re_x^{-1/2}Nu_x$ are accelerated with the rise of φ_2. These physical quantities are higher for Al_2O_3-Cu/water ($\varphi_1 = 0.05$) rather than that Cu/water ($\varphi_1 = 0$). Besides, the reduction of $Re_x^{1/2}C_f$ and the increment of $Re_x^{-1/2}Nu_x$ are observed for larger λ, in the range of $-0.5 \leq \lambda \leq 0.5$. Additionally, the values of $Re_x^{1/2}C_f$ and $Re_x^{-1/2}Nu_x$ for Cu/water ($\varphi_1 = 0, \varphi_2 = 0.05$) when $\lambda = -0.5, 0, 0.5$ are comparable to those obtained by Waini et al. [26].

Figs. 2 and 3 illustrate the variations of $Re_x^{1/2}C_f$ and $Re_x^{-1/2}Nu_x$ against λ for $\varphi_2 = 0, 0.03, 0.05$ when $\varphi_1 = 0.05$ and Pr = 6.2. Results show that as φ_2 increases, the friction on the surface is increased for $\lambda < 1$, while it is decreased for $\lambda > 1$, and no friction occurs when $\lambda = 1$.

Table 3

Values of $f''(0)$ with different λ for regular fluid.($\varphi_1 = \varphi_2 = 0$).

λ	Wang [4]	Bachok et al. [6]	Present results
2	−1.88731	−1.887307	−1.887307
1	0	0	0
0.5	0.71330	0.713295	0.713295
0	1.232588	1.232588	1.232588
−0.5	1.49567	1.495670	1.495670
−1	1.32882	1.328817	1.328817
−1.15	1.08223	1.082231	1.082231
	[0.116702]	[0.116702]	[0.116702]
−1.2		0.932473	0.932473
		[0.233650]	[0.233650]
−1.2465	0.55430	0.584281	0.584281
		[0.554297]	[0.554296]

Note: [ ] Second solution.

Table 4
Values of $Re_x^{1/2}C_f$ and $Re_x^{-1/2}Nu_x$ for various values of φ_1, φ_2 and λ.

φ_2	λ	$\varphi_1 = 0$(Cu/water)		$\varphi_1 = 0.05$(Al$_2$O$_3$-Cu/water)	
		$Re_x^{1/2}C_f$	$Re_x^{-1/2}Nu_x$	$Re_x^{1/2}C_f$	$Re_x^{-1/2}Nu_x$
0	0	1.232588	1.127964	1.408763	1.229275
0.03		1.425110	1.213918	1.605715	1.317395
0.05		1.553850	1.269379	1.738637	1.374810
0.05	−0.5	1.885501	0.706314	2.109729	0.791231
		[1.885501]	[0.706314]		
	0	1.553850	1.269379	1.738637	1.374810
		[1.553850]	[1.269379]		
	0.5	0.899208	1.733859	1.006144	1.856885
		[0.899208]	[1.733859]		

Note: [ ] Results by Waini et al. [26].
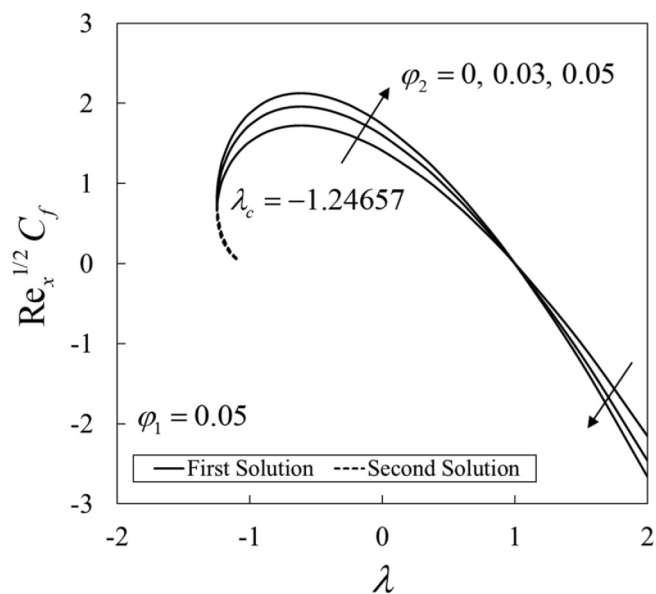
Fig. 2. The variation of $Re_x^{1/2}C_f$ against λ for various values of φ_2.
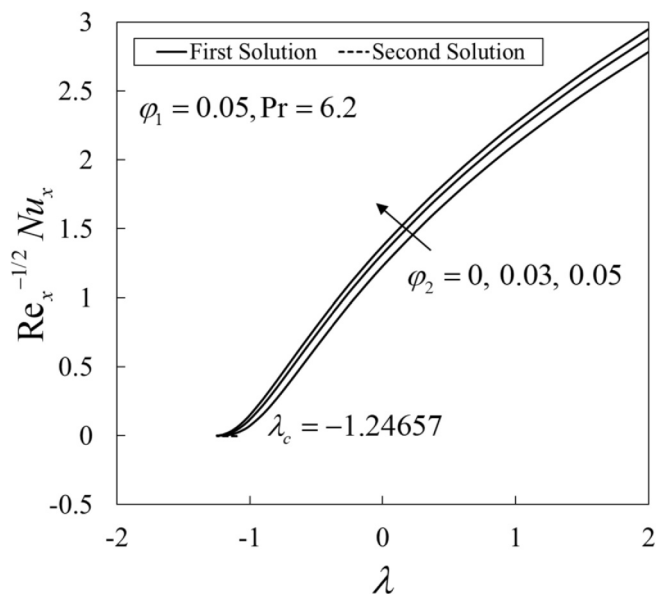
Fig. 3. The variation of $Re_x^{-1/2}Nu_x$ against λ for various values of φ_2.
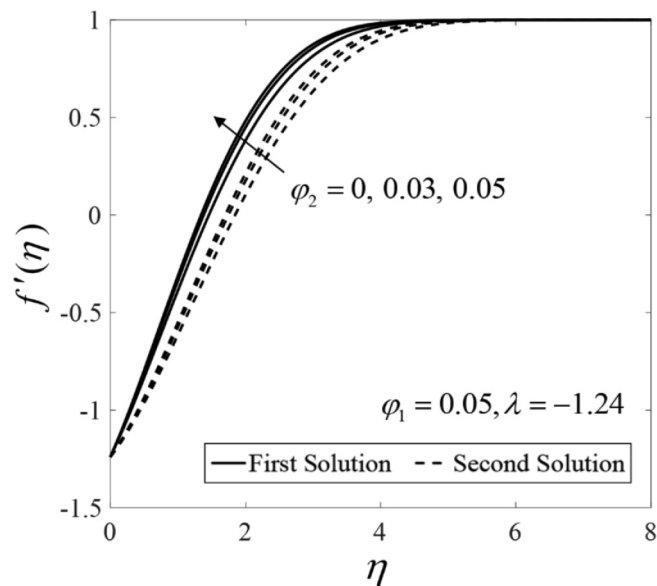
Fig. 4. Effect of φ_2 on $f'(\eta)$.
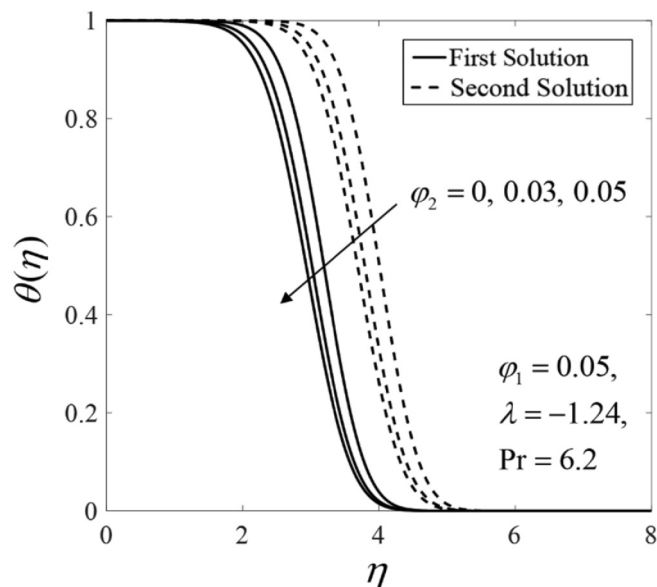
Fig. 5. Effect of φ_2 on $\theta(\eta)$.

Besides, the heat transfer rate is intensified with the rising of φ_2. From the numerical computations, the non-uniqueness of the solutions are found for the shrinking case, in the range of $-1.24657 < \lambda \le -1.1$ with $\lambda_c = -1.24657$ is the point of bifurcation between the solutions. Meanwhile, the solution is unique for $\lambda > -1.1$.

On the other hand, Figs. 4 and 5 provides the velocity $f'(\eta)$ and the temperature $\theta(\eta)$ profiles for $\varphi_2 = 0, 0.03, 0.05$ when $\varphi_1 = 0.05$, $\lambda = -1.24$, and Pr = 6.2. Results show that the increase in φ_2 inclines the velocity profiles $f'(\eta)$ for both solution branches, however, it reduces the temperature profiles $\theta(\eta)$. Besides, Figs. 6 and 7 show the effect of λ on $f'(\eta)$ and $\theta(\eta)$ when $\varphi_1 = \varphi_2 = 0.05$ and Pr = 6.2. It is seen that the first and second solutions of $f'(\eta)$ and $\theta(\eta)$ are getting closer to each other for smaller λ. These solutions are merged at a critical value of λ, i.e $\lambda_c = -1.24657$ where they are terminated.

The variations of γ against λ when $\varphi_1 = \varphi_2 = 0.05$ is portrayed in Fig. 8. The solution's stability is subjected to the sign of γ as described by the perturbation function, given in Eq. (17). For the positive value of γ, $e^{-\gamma\tau} \to 0$ when $\tau \to \infty$. Meanwhile, the negative value of γ gives

Fig. 6. Effect of λ on $f'(\eta)$.

Fig. 8. The variation of γ against λ.
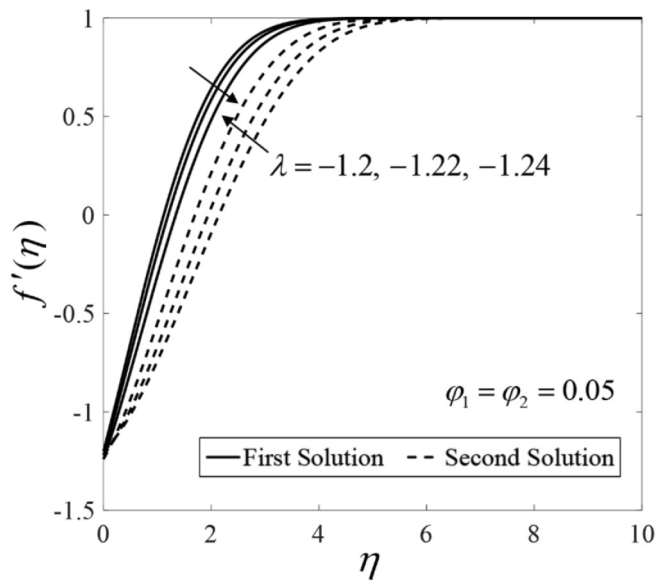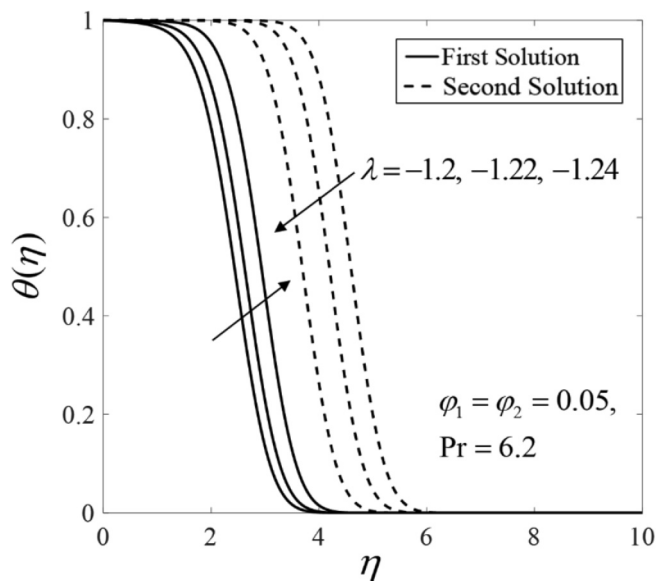
Fig. 7. Effect of λ on $\theta(\eta)$.

$e^{-\gamma\tau} \to \infty$ when $\tau \to \infty$. These behaviours show that the solution converges and in a stable mode for the first solution. However, the solution diverges and in an unstable mode for the second solution.

Conclusions

The Hiemenz flow on a shrinking surface containing hybrid nanoparticle (Al$_2$O$_3$-Cu) was accomplished. The impact of several physical parameters on the behaviour of the flow was examined. It was revealed that the solutions are not unique for a certain range of the shrinking strength, i.e. $-1.24657 < \lambda \le -1.1$, whereas the solution is unique for $\lambda > -1.1$. The bifurcation between the first and the second solutions occurred at $\lambda_c = -1.24657$ for all values of φ_2 considered. Meanwhile, the heat transfer rate intensified with φ_2. Moreover, as φ_2 increased, the increment of the friction on the surface was observed for $\lambda < 1$, while it decreased for $\lambda > 1$, and no friction at the fluid–solid interface when $\lambda = 1$. The first and second solutions of $f'(\eta)$ and $\theta(\eta)$ merged and terminated at $\lambda_c = -1.24657$. Lastly, the temporal stability of the dual solutions was tested where the results showed that the first solution is stable in the long run.
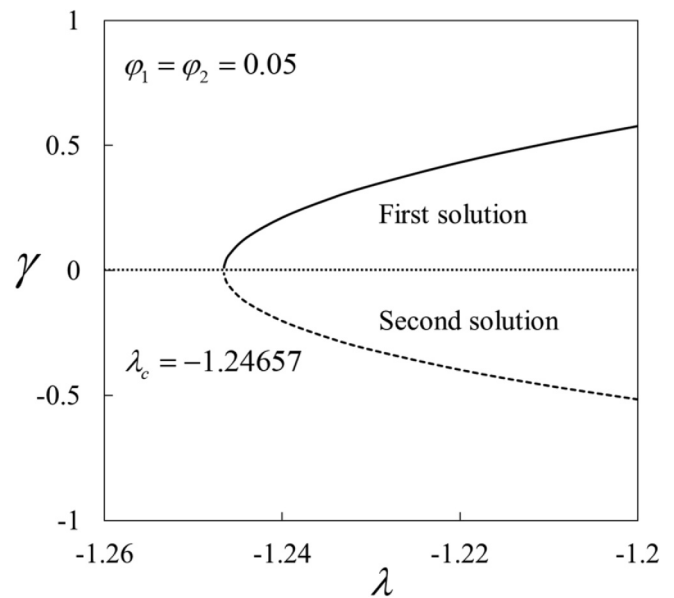
Author statement

IP and AI formulate the problem. IW performs the numerical computation. All authors contribute equally in writing the paper.

References

[1] Hiemenz K. Die Grenzschicht an einem in den gleichförmigen Flüssigkeitsstrom eingetauchten geraden Kreiszylinder. Dinglers Polytech J 1911;326:321–410.
[2] Der HF. Einfluß grober Zähigkeit bei der Strömung um den Zylinder und um die Kugel. Zeitschrift Für Angew Math Und Mech 1936;16:153–64.
[3] Ariel PD. Hiemenz flow in hydromagnetics. Acta Mech 1994;103:31–43.
[4] Wang CY. Stagnation flow towards a shrinking sheet. Int J Non Linear Mech 2008;43:377–82.
[5] Ishak A, Lok YY, Pop I. Stagnation-point flow over a shrinking sheet in a micropolar fluid. Chem Eng Commun 2010;197:1417–27.
[6] Bachok N, Ishak A, Pop I. Stagnation-point flow over a stretching/shrinking sheet in a nanofluid. Nanoscale Res Lett 2011;6. Article ID 623.
[7] Dholey S. An unsteady separated stagnation-point flow towards a rigid flat plate. J Fluids Eng 2019;141. Article ID 021202.
[8] Fang T, Wang F, Gao B. Unsteady magnetohydrodynamic stagnation point flow — closed-form analytical solutions. Appl Math Mech (Engl Ed) 2019;40:449–64.
[9] Weidman P. Hiemenz stagnation-point flow impinging on a biaxially stretching surface. Meccanica 2018;53:833–40.
[10] Weidman P. Hiemenz stagnation-point flow impinging on a uniformly rotating plate. Eur J Mech B/Fluids 2019;78:169–73.
[11] Choi SUS, Eastman JA. Enhancing thermal conductivity of fluids with nanoparticles. Proc 1995 ASME Int Mech Eng Congr Expo FED 231/MD 1995;66:99–105.
[12] Khanafer K, Vafai K, Lightstone M. Buoyancy-driven heat transfer enhancement in a two-dimensional enclosure utilizing nanofluids. Int J Heat Mass Transf 2003;46:3639–53.

[13] Tiwari RK, Das MK. Heat transfer augmentation in a two-sided lid-driven differentially heated square cavity utilizing nanofluids. Int J Heat Mass Transf 2007;50:2002–18.

[14] Oztop HF, Abu-Nada E. Numerical study of natural convection in partially heated rectangular enclosures filled with nanofluids. Int J Heat Fluid Flow 2008;29:1326–36.

[15] Mohebbi R, Rashidi MM. Numerical simulation of natural convection heat transfer of a nanofluid in an L-shaped enclosure with a heating obstacle. J Taiwan Inst Chem Eng 2017;72:70–84.

[16] Gavili A, Isfahani T. Experimental investigation of transient heat transfer coefficient in natural convection with Al2O3-nanofluids. Heat Mass Transf 2020;56:901–11.

[17] Turkyilmazoglu M. Single phase nanofluids in fluid mechanics and their hydrodynamic linear stability analysis. Comput Methods Programs Biomed 2020;187. Article ID 105171.

[18] Turcu R, Darabont A, Nan A, Aldea N, Macovei D, Bica D, et al. New polypyrrole-multiwall carbon nanotubes hybrid materials. J Optoelectron Adv Mater 2006;8:643–7.

[19] Jana S, Salehi-Khojin A, Zhong WH. Enhancement of fluid thermal conductivity by the addition of single and hybrid nano-additives. Thermochim Acta 2007;462:45–55.

[20] Suresh S, Venkitaraj KP, Selvakumar P, Chandrasekar M. Synthesis of Al2O3-Cu/water hybrid nanofluids using two step method and its thermo physical properties. Colloids Surfaces A Physicochem Eng Asp 2011;388:41–8.

[21] Devi SPA, Devi SSU. Numerical investigation of hydromagnetic hybrid Cu- Al2O3/water nanofluid flow over a permeable stretching sheet with suction. Int J Nonlinear Sci Numer Simul 2016;17:249–57.

[22] Ghalambaz M, Rosca NC, Rosca AV, Pop I. Mixed convection and stability analysis of stagnation-point boundary layer flow and heat transfer of hybrid nanofluids over a vertical plate. Int J Numer Meth Heat Fluid Flow 2020;30:3737–54.

[23] Hassan M, Faisal A, Ali I, Bhatti MM, Yousaf M. Effects of Cu–Ag hybrid nanoparticles on the momentum and thermal boundary layer flow over the wedge. Proc Inst Mech Eng Part E J Process Mech Eng 2019;233:1128–36.

[24] Mahanthesh B, Shehzad SA, Ambreen T, Khan SU. Significance of Joule heating and viscous heating on heat transport of MoS2–Ag hybrid nanofluid past an isothermal wedge. J Therm Anal Calorim 2020. https://doi.org/10.1007/s10973-020-09578-y.

[25] Waini I, Ishak A, Pop I. Unsteady flow and heat transfer past a stretching/shrinking sheet in a hybrid nanofluid. Int J Heat Mass Transf 2019;136:288–97.

[26] Waini I, Ishak A, Pop I. MHD flow and heat transfer of a hybrid nanofluid past a permeable stretching/shrinking wedge. Appl Math Mech (English Ed) 2020;41:507–20.

[27] Waini I, Ishak A, Groşan T, Pop I. Mixed convection of a hybrid nanofluid flow along a vertical surface embedded in a porous medium. Int Commun Heat Mass Transf 2020;114. Article ID 104565.

[28] Waini I, Ishak A, Pop I. Hybrid nanofluid flow towards a stagnation point on an exponentially stretching/shrinking vertical sheet with buoyancy effects. Int J Numer Meth Heat Fluid Flow 2020. https://doi.org/10.1108/HFF-02-2020-0086.

[29] Waini I, Ishak A, Pop I. Hybrid nanofluid flow towards a stagnation point on a stretching/shrinking cylinder. Sci Rep 2020;10. Article ID 9296.

[30] Ghadikolaei SS, Yassari M, Sadeghi H, Hosseinzadeh K, Ganji DD. Investigation on thermophysical properties of TiO2–Cu/H2O hybrid nanofluid transport dependent on shape factor in MHD stagnation point flow. Powder Technol 2017;322:428–38.

[31] Jamshed W, Aziz A. Cattaneo-Christov based study of TiO2–CuO/EG Casson hybrid nanofluid flow over a stretching surface with entropy generation. Appl Nanosci 2018;8:685–98.

[32] Hayat T, Nadeem S, Khan AU. Rotating flow of Ag-CuO/H2O hybrid nanofluid with radiation and partial slip boundary effects. Eur Phys J E 2018;41. Article ID 75.

[33] Subhani M, Nadeem S. Numerical analysis of micropolar hybrid nanofluid. Appl Nanosci 2019;9:447–59.

[34] Maskeen MM, Zeeshan A, Mehmood OU, Hassan M. Heat transfer enhancement in hydromagnetic alumina–copper/water hybrid nanofluid flow over a stretching cylinder. J Therm Anal Calorim 2019;138:1127–36.

[35] Nadeem S, Abbas N, Khan AU. Characteristics of three dimensional stagnation point flow of hybrid nanofluid past a circular cylinder. Results Phys 2018;8:829–35.

[36] Hayat T, Nadeem S. Heat transfer enhancement with Ag–CuO/water hybrid nanofluid. Results Phys 2017;7:2317–24.

[37] Sheikholeslami M, Ganji DD. Nanofluid convective heat transfer using semi analytical and numerical approaches: a review. J Taiwan Inst Chem Eng 2016;65:43–77.

[38] Myers TG, Ribera H, Cregan V. Does mathematics contribute to the nanofluid debate? Int J Heat Mass Transf 2017;111:279–88.

[39] Khanafer K, Vafai K. Applications of nanofluids in porous medium a critical review. J Therm Anal Calorim 2019;135:1479–92.

[40] Farhana K, Kadirgama K, Rahman MM, Noor MM, Ramasamy D, Samykano M, et al. Significance of alumina in nanofluid technology: an overview. J Therm Anal Calorim 2019;138:1107–26.

[41] Sarkar J, Ghosh P, Adil A. A review on hybrid nanofluids: recent research, development and applications. Renew Sustain Energy Rev 2015;43:164–77.

[42] Sidik NAC, Adamu IM, Jamil MM, Kefayati GHR, Mamat R, Najafi G. Recent progress on hybrid nanofluids in heat transfer applications: a comprehensive review. Int Commun Heat Mass Transf 2016;78:68–79.

[43] Sundar LS, Sharma KV, Singh MK, Sousa ACM. Hybrid nanofluids preparation, thermal properties, heat transfer and friction factor – a review. Renew Sustain Energy Rev 2017;68:185–98.

[44] Babu JAR, Kumar KK, Rao SS. State-of-art review on hybrid nanofluids. Renew Sustain Energy Rev 2017;77:551–65.

[45] Ahmadi MH, Mirlohi A, Alhuyi Nazari M, Ghasempour R. A review of thermal conductivity of various nanofluids. J Mol Liq 2018;265:181–8.

[46] Huminic G, Huminic A. Hybrid nanofluids for heat transfer applications – a state-of-the-art review. Int J Heat Mass Transf 2018;125:82–103.

[47] Huminic G, Huminic A. Entropy generation of nanofluid and hybrid nanofluid flow in thermal systems: a review. J Mol Liq 2020;302. Article ID 112533.

[48] Abbas IA, Marin M. Analytical solution of thermoelastic interaction in a half-space by pulsed laser heating. Phys E Low-Dimensional Syst Nanostructures 2017;87:254–60.

[49] Abd-Elaziz EM, Marin M, Othman MIA. On the effect of thomson and initial stress in a thermo-porous elastic solid under G-N electromagnetic theory. Symmetry 2019;11. Article ID 413.

[50] Riaz A, Ellahi R, Bhatti MM, Marin M. Study of heat and mass transfer in the eyring-powell model of fluid propagating peristaltically through a rectangular compliant channel. Heat Transf Res 2019;50:1539–60.

[51] White FM. Viscous Fluid Flow. 3rd ed. New York: McGraw-Hill; 2006.

[52] Schlichting H, Gersten K. Boundary Layer Theory. 8th ed. Berlin: Springer; 2003.

[53] Merkin JH. On dual solutions occurring in mixed convection in a porous medium. J Eng Math 1986;20:171–9.

[54] Weidman PD, Kubitschek DG, Davis AMJ. The effect of transpiration on self-similar boundary layer flow over moving surfaces. Int J Eng Sci 2006;44:730–7.

[55] Harris SD, Ingham DB, Pop I. Mixed convection boundary-layer flow near the stagnation point on a vertical surface in a porous medium: Brinkman model with slip. Transp Porous Media 2009;77:267–85.

[56] Shampine LF, Gladwell I, Thompson S. Solving ODEs with MATLAB. Cambridge: Cambridge University Press; 2003.